A finite element mixture model for hierarchical porous media

INTERNATIONAL JOURNAL FOR NUMERICAL METHODS IN ENGINEERING, VOL. 40, 193–210 (1997)

A FINITE ELEMENT MIXTURE MODEL FOR HIERARCHICAL POROUS MEDIA

W. J. VANKAN, J. M. HUYGHE*, M. R. DROST*, J. D. JANSSEN* AND A. HUSON*

Department of Mechanical Engineering, Eindhoven University of Technology, P.O. Box 513, 5600 MB Eindhoven, The Netherlands

SUMMARY

A finite element description of fluid flow through a deforming porous solid, with a hierarchical structure of pores, has been developed and implemented in the finite element software package DIANA.[1] Several standard element types can be used for 2-D, axisymmetric and 3-D finite deformation analysis. The hierarchy is dealt with as an extra dimension, quantified by a parameter x_0. Both spatial and hierarchical fluid flow is described by a Darcy equation. Fluid pressure and hydrostatic solid pressure are related via an elastic fluid–solid interface. The state of the fluid, the Darcy permeability tensor and the elastic interface depend on both spatial position and hierarchical level. Discretization and integration of fluid related quantities are split into a spatial and a hierarchical part. The degrees of freedom of the finite element model are the displacements of the solid, the hydrostatic pressure and a number of fluid pressures on different hierarchical levels.

Blood-perfused biological tissue can be regarded as a hierarchical porous solid, where the fluid represents the blood and the hierarchy corresponds to the tree-like vascular structure. As an example, a simulation of a contracting, blood-perfused skeletal muscle is presented.

KEY WORDS: finite deformation; mixture theory; blood-perfusion; muscle; contraction

1. INTRODUCTION

Blood perfusion is a complex and sophisticated mechanism of nutrition and drainage of biological tissues. Some of these tissues are subject to large mechanical loads and deformations. Mechanical processes in the tissue can significantly interact with blood perfusion.[2, 3] In order to investigate these mechanical processes and interactions, the material behaviour of the tissue can be mathematically modelled by means of the mixture theory.[4, 5]

Blood-perfused biological tissue can be described as a mixture, in which the fluid phase represents the blood and the surrounding tissue is represented by the solid. The blood vessels can be regarded as pores in the solid. An essential aspect of vasculature is its hierarchical architecture: the blood flows from one or a few large supplying arteries through a diverging, arteriolar vascular bed (Figure 1), reaches the capillaries, and is drained by a converging venous vasculature. In the greater part of the hierarchy, vessels are numerous and lie homogeneously distributed in the tissue. Within each small and bounded spatial region in the tissue (averaging volume in mixture theory), we therefore distinguish between blood that resides in the different parts of the hierarchy. Vascular properties, like vessel diameter, wall thickness and stiffness, vessel orientation and vessel

*Department of Movement Sciences, University of Limburg, P.O. Box 616, 6200 MD Maastricht, The Netherlands

CCC 0029–5981/97/020193–18

Received 2 June 1995
Revised 18 December 1995

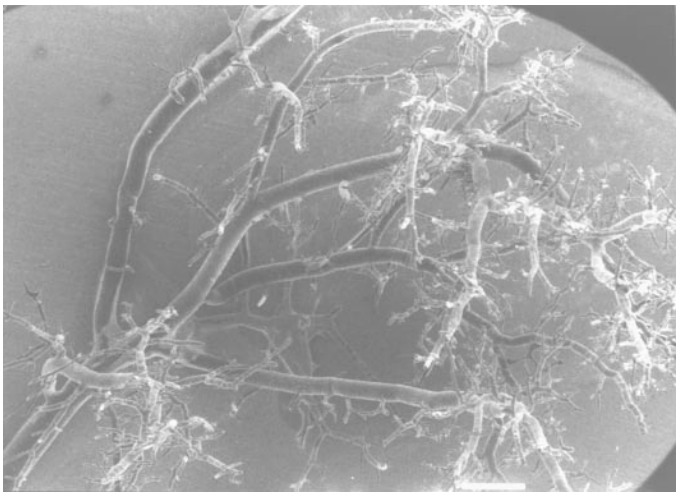

Figure 1. Scanning electron micrograph of a polymer cast of the arterial part of a vascular tree. A large supplying arterial vessel ($d \approx 0{\cdot}5$ mm) can be observed, from which many smaller vessels bifurcate. The smallest vessels that were reached by the polymer are arterioles ($d \approx 50\,\mu$m). In reality, from these vessels smaller and smaller arteriolar vessels bifurcate, whereafter the capillary vessels are reached ($d \approx 5\,\mu$m), which run towards the converging venous bed. The small white line on the right-hand side at the bottom of the photograph represents a distance of 1 mm

density of the tissue, vary over the hierarchy. Consequently, the state of the blood is a function of its position in the hierarchy. Therefore, blood pressure and flow should, apart from their spatial dependency, also be specified by a hierarchical dependency. Moreover, the vessel walls, which form an elastic interface between the blood and the extravascular tissue, should be described as a function of hierarchical position.

A description of biphasic mixtures, which consist of one solid and one fluid, was derived by Biot.[6] We extended this biphasic theory for application to blood perfusion.[7, 8] The extended theory describes the state of the fluid phase as a continuous function of both spatial and hierarchical position. Just like in the biphasic mixture theory, the flow of the fluid is described by a Darcy equation. In the extended theory however, this Darcy equation includes flow components in the hierarchical direction, by which the communication of blood between the different compartments in the vasculature is described.[9] Huyghe *et al.*[10] illustrated the applicability of this extended theory to Newtonian flow through a rigid vascular network. In the present study a finite element formulation has been derived for the extended theory, which includes finite deformation of the tissue and elasticity of the vessel walls. Galerkin's method has been used to transform the discretized weighted residual equations to their finite element form. The resulting nodal degrees of freedom are the displacements of the solid, the mixture's hydrostatic pressure and a number of fluid pressures representing the different pressures in the hierarchy. Special attention was paid to the discretization of the fluid pressure because of its dependency on both space and hierarchical position. Although this mixture description is specifically developed for biological materials, its applicability to technical materials, such as for example cracked rocks and soils, is not excluded.

The finite element model has been implemented in the finite element software package DIANA[1] (DIANA Analysis bv, P.O. Box 113, 2600 AC Delft, The Netherlands). As an illustration of the possibilities of the model, some results of a simulation with the model of a blood-perfused, contracting skeletal muscle are presented.

2. MATERIAL BEHAVIOUR

2.1. Conservation of mass and momentum

The equations of conservation of mass and momentum for a hierarchical mixture can be derived from the ordinary conservation equations of constituents of mixtures, which read in their quasi-static local form and under the assumption of intrinsic incompressibility of each constituent:[11]

$$\text{mass: } \frac{\partial n^\alpha}{\partial t} + \boldsymbol{\nabla} \cdot (n^\alpha \mathbf{v}^\alpha) = \theta^\alpha, \quad \alpha = 1, \ldots, \nu \tag{1}$$

$$\text{momentum: } \boldsymbol{\nabla} \cdot \boldsymbol{\sigma}^\alpha + \boldsymbol{\pi}^\alpha = \mathbf{0}, \quad \alpha = 1, \ldots, \nu \tag{2}$$

where t is time, n^α is the volume fraction, $\mathbf{v}^\alpha$ the velocity, $\boldsymbol{\sigma}^\alpha$ the Cauchy stress tensor and θ^α and $\boldsymbol{\pi}^\alpha$ are the volume and momentum interaction of constituent α. It is assumed that there is no exchange of moment of momentum among the constituents, so that $\boldsymbol{\sigma}^\alpha$ is symmetric. A hierarchical mixture consists of one solid constituent and a fluid constituent that is subdivided into a continuous series of fluid compartments. The positions of the fluid compartments in the hierarchy are specified by a parameter x_0, which will be interpreted as an extra independent dimension. Each compartment represents the fluid that resides in the part $[x_0, x_0 + \mathrm{d}x_0]$ of the hierarchical range, and is treated as a separate constituent. Communication between the compartments is described by the fluid volume interaction term $\tilde{\theta}^{\mathrm{f}}$:

$$\tilde{\theta}^{\mathrm{f}} = -\frac{\partial(\tilde{n}^{\mathrm{f}} \tilde{v}_0^{\mathrm{f}})}{\partial x_0}; \quad \tilde{v}_0^{\mathrm{f}} = \frac{\mathrm{D}x_0}{\mathrm{D}t} \tag{3}$$

$\tilde{n}^{\mathrm{f}} \tilde{v}_0^{\mathrm{f}}$ represents the fluid flux from one compartment to the next per unit volume of mixture. Thus, $\tilde{\theta}^{\mathrm{f}}$ can be physically interpreted as the difference between the fluid flux from the previous compartment and the fluid flux to the next compartment. $\tilde{\theta}^{\mathrm{f}}$ and $\tilde{n}^{\mathrm{f}}$ are measured per unit x_0 and per unit volume of mixture. As we ensure that no fluid is assigned an x_0-value outside the range $[0, 1]$, we require the boundary conditions: $\tilde{v}_0^{\mathrm{f}}(x_0, \mathbf{x}) = 0$; $x_0 = 0, x_0 = 1$; $\forall \mathbf{x}$. Throughout this paper the exponents s and f are used to indicate solid and fluid, respectively, and a tilde ($\tilde{}$) is used to indicate that a quantity depends on x_0 and, if the quantity is volume specific, is defined per unit x_0.

Equations (1) and (2) yield for conservation of the hierarchical mixture:

$$\text{solid mass: } -\frac{\partial n^{\mathrm{f}}}{\partial t} + \boldsymbol{\nabla} \cdot ((1 - n^{\mathrm{f}}) \mathbf{v}^{\mathrm{s}}) = 0 \tag{4}$$

$$\text{fluid mass: } \frac{\partial \tilde{n}^{\mathrm{f}}}{\partial t} + {}_4\boldsymbol{\nabla} \cdot (\tilde{n}^{\mathrm{f}} {}_4\tilde{\mathbf{v}}^{\mathrm{f}}) = 0 \tag{5}$$

$$\text{momentum: } \boldsymbol{\nabla} \cdot \boldsymbol{\sigma}^{\mathrm{s}} + \int_0^1 \boldsymbol{\nabla} \cdot \tilde{\boldsymbol{\sigma}}^{\mathrm{f}} \, \mathrm{d}x_0 = \mathbf{0} \tag{6}$$

where use has been made of the assumption of saturation

$$n^{\mathrm{s}} + \int_0^1 \tilde{n}^{\mathrm{f}} \mathrm{d}x_0 = n^{\mathrm{s}} + n^{\mathrm{f}} = 1 \tag{7}$$

and the four-dimensional operator ${}_4\boldsymbol{\nabla}$ and vector ${}_4\tilde{\mathbf{v}}^{\mathrm{f}}$, in which x_0 components are included:

$$ {}_4\boldsymbol{\nabla} = \left\{ \begin{array}{c} \dfrac{\partial}{\partial x_0} \\ \boldsymbol{\nabla} \end{array} \right\}, \quad {}_4\tilde{\mathbf{v}}^{\mathrm{f}} = \left\{ \begin{array}{c} \tilde{v}_0^{\mathrm{f}} \\ \tilde{\mathbf{v}}^{\mathrm{f}} \end{array} \right\} \tag{8} $$

2.2. Constitutive behaviour

The constitutive behaviour of the hierarchical mixture can be derived by applying the first law of thermodynamics, conservation of energy, of each constituent to the entropy inequality of the total mixture.[11] By choosing the Green–Lagrange strain tensor $\mathbf{E}$, the Lagrangian form of the fluid volume fraction $J\tilde{n}^{\mathrm{f}}$, and the relative velocity ${}_4\tilde{\mathbf{v}}^{\mathrm{fs}}$ as independent variables in the description of the mixture's constitutive behaviour, the following constitutive relations for effective stress and the relative volumetric flux of the fluid can be found, respectively:

$$ \boldsymbol{\sigma}^{\mathrm{eff}} = \frac{1}{J}\mathbf{F} \cdot \frac{\partial W}{\partial \mathbf{E}} \cdot \mathbf{F}^{\mathrm{c}} \tag{9} $$

$$ \tilde{n}^{\mathrm{f}}\, {}_4\tilde{\mathbf{v}}^{\mathrm{fs}} = -{}_4\tilde{\mathbf{K}} \cdot {}_4\boldsymbol{\nabla}_0 \tilde{\mu}^{\mathrm{f}} \tag{10} $$

where J is the relative volume change and W is the strain energy function of the mixture. ${}_4\tilde{\mathbf{K}}$ is the four-dimensional permeability tensor and ${}_4\tilde{\mathbf{v}}^{\mathrm{fs}}$ is the four-dimensional vector of the relative fluid velocity:

$$ {}_4\tilde{\mathbf{K}} = \left[\begin{array}{cc} \tilde{k}_{00} & \tilde{\mathbf{k}}_0 \\ \tilde{\mathbf{k}}_0 & \tilde{\mathbf{K}} \end{array} \right], \quad {}_4\tilde{\mathbf{v}}^{\mathrm{fs}} = \left\{ \begin{array}{c} \tilde{v}_0^{\mathrm{f}} \\ \mathbf{F}^{-1} \cdot (\tilde{\mathbf{v}}^{\mathrm{f}} - \mathbf{v}^{\mathrm{s}}) \end{array} \right\} \tag{11} $$

in which $\mathbf{F}$ is the deformation tensor. Equation (10) is known as the Darcy equation,[6] in which $\tilde{\mu}^{\mathrm{f}}$ is the chemical potential of the fluid, defined as

$$ \tilde{\mu}^{\mathrm{f}} = \frac{\partial \tilde{W}}{\partial (J\tilde{n}^{\mathrm{f}})} + p \tag{12} $$

which represents the fluid pressure. The effective stress $\boldsymbol{\sigma}^{\mathrm{eff}}$ in (9) is defined as the deformation dependent part of the total stress in the mixture:

$$ \boldsymbol{\sigma}^{\mathrm{eff}} = \boldsymbol{\sigma}^{\mathrm{s}} + \int_0^1 \tilde{\boldsymbol{\sigma}}^{\mathrm{f}} \, \mathrm{d}x_0 + p\mathbf{I} \tag{13} $$

where p represents the mixture's hydrostatic pressure.

A more detailed description of the derivation of the conservation equations and constitutive restrictions is given in Reference 12. Similar conservation equations and constitutive behaviour were found by Huyghe and van Campen,[7, 8] who used a formal averaging procedure in their derivation.

3. NUMERICAL SOLUTION METHOD

3.1. Weighted residual formulation

The hierarchical mixture description has been implemented in the finite element software package DIANA. For this purpose the expression of the effective stress (13) is substituted into the equation

of conservation of momentum (6), the equation of conservation of solid mass (4) is used as such, and the extended Darcy equation (10) is substituted into the equation of conservation of fluid mass (5). Thus, the system of differential equations results in:

$$\text{momentum: } \boldsymbol{\nabla} \cdot \boldsymbol{\sigma}^{\text{eff}} - \boldsymbol{\nabla} p = \mathbf{0} \tag{14}$$

$$\text{solid: } -\frac{\partial n^{\text{f}}}{\partial t} + \boldsymbol{\nabla} \cdot ((1 - n^{\text{f}})\mathbf{v}^{\text{s}}) = 0 \tag{15}$$

$$\text{fluid: } \frac{\partial \tilde{n}^{\text{f}}}{\partial t} + {}_4\boldsymbol{\nabla} \cdot (-{}_4\mathbf{F} \cdot {}_4\tilde{\mathbf{K}} \cdot {}_4\boldsymbol{\nabla}_0 \tilde{\mu}^{\text{f}} + \tilde{n}^{\text{f}}{}_4\mathbf{v}^{\text{s}}) = 0 \tag{16}$$

The finite element formulation of this system of equations is obtained by using the weighted residual method.[13] The weighted residual form of the momentum equation (14) is applied to an actual volume V of mixture with surrounding surface A:

$$\int_V \mathbf{f} \cdot (\boldsymbol{\nabla} \cdot (\boldsymbol{\sigma}^{\text{eff}} - p\mathbf{I}))\,\mathrm{d}V = \mathbf{0} \tag{17}$$

which, by applying Gauss' theorem, can be transformed to

$$\int_V (\boldsymbol{\nabla}\mathbf{f})^{\text{c}} : (\boldsymbol{\sigma}^{\text{eff}} - p\mathbf{I})\,\mathrm{d}V = -\int_A \mathbf{f} \cdot \mathbf{a}\,\mathrm{d}A \tag{18}$$

Here $\mathbf{f}$ is an arbitrary vector function defined in V, $\mathbf{a} = -(\boldsymbol{\sigma}^{\text{eff}} - p\mathbf{I}) \cdot \mathbf{n}$ is the external load applied to A and $\mathbf{n}$ is the outer normal on A. Equation (18) is transformed to the undeformed configuration, with reference volume V_0 and surrounding surface A_0 with normal $\mathbf{n}_0$:

$$\int_{V_0} (\boldsymbol{\nabla}_0\mathbf{f})^{\text{c}} : (\mathbf{S} \cdot \mathbf{F}^{\text{c}} - pJ\mathbf{F}^{-1})\,\mathrm{d}V_0 = -\int_{A_0} J\mathbf{f} \cdot \mathbf{F}^{-\text{c}} \cdot \mathbf{a}_0\,\mathrm{d}A_0 \tag{19}$$

where $\mathbf{a}_0 = -(\boldsymbol{\sigma}^{\text{eff}} - p\mathbf{I}) \cdot \mathbf{n}_0$ and the second Piola–Kirchhoff stress tensor, which is defined as $\mathbf{S} = J\mathbf{F}^{-1} \cdot \boldsymbol{\sigma}^{\text{eff}} \cdot \mathbf{F}^{-\text{c}}$, are used. The exponent c denotes the conjugate of a tensor.

Conservation of solid mass (4) is transformed to a more suitable form by employing the identity $\boldsymbol{\nabla} \cdot \mathbf{v}^{\text{s}} = (\mathrm{D}^{\text{s}} J / \mathrm{D}t)/J$:

$$-\frac{1}{J}\frac{\mathrm{D}^{\text{s}}}{\mathrm{D}t}(Jn^{\text{f}}) + \boldsymbol{\nabla} \cdot \mathbf{v}^{\text{s}} = 0 \tag{20}$$

The weighted residual form of (20) is applied to a volume V of mixture with surrounding surface A, and the expression for n^{f} according to (7) is substituted:

$$\int_V g\left(-\frac{1}{J}\frac{\mathrm{D}^{\text{s}}}{\mathrm{D}t}\left(J\int_0^1 \tilde{n}^{\text{f}}\,\mathrm{d}x_0\right) + \boldsymbol{\nabla} \cdot \mathbf{v}^{\text{s}}\right)\mathrm{d}V = 0 \tag{21}$$

where g is an arbitrary scalar function defined in V. The strain energy function W of the mixture is assumed to depend on the solid deformation via the strain tensor $\mathbf{E}$ and on the chemical potential $\tilde{\mu}^{\text{f}}$ via the fluid volume fraction $J\tilde{n}^{\text{f}}$ (equation (12)). Furthermore, assuming $J\tilde{n}^{\text{f}}$ to depend only on $(\tilde{\mu}^{\text{f}} - p)$ and transforming (21) to the reference configuration yields

$$\int_{V_0} g\left(-\int_0^1 \frac{\partial(J\tilde{n}^{\text{f}})}{\partial(\tilde{\mu}^{\text{f}} - p)}\frac{\mathrm{D}^{\text{s}}}{\mathrm{D}t}(\tilde{\mu}^{\text{f}} - p)\,\mathrm{d}x_0 + J\mathbf{F}^{-\text{c}} \cdot \boldsymbol{\nabla}_0 \cdot \mathbf{v}^{\text{s}}\right)\mathrm{d}V_0 = 0 \tag{22}$$

where

$$\frac{\partial(J\tilde{n}^{\mathrm{f}})}{\partial(\tilde{\mu}^{\mathrm{f}}-p)}=\frac{1}{\dfrac{\partial^2 W}{\partial(J\tilde{n}^{\mathrm{f}})^2}} \tag{23}$$

Similar to conservation of solid mass, conservation of fluid mass (16) is transformed to a suitable form:

$$\frac{1}{J}\frac{\mathrm{D}^{\mathrm{s}}}{\mathrm{D}t}(J\tilde{n}^{\mathrm{f}})-{}_4\boldsymbol{\nabla}\cdot({}_4\mathbf{F}\cdot{}_4\tilde{\mathbf{K}}\cdot{}_4\boldsymbol{\nabla}_0\tilde{\mu}^{\mathrm{f}})=0 \tag{24}$$

The weighted residual form of equation (24) is applied to a volume V of mixture with surrounding surface A, containing the total hierarchical range:

$$\int_V\int_0^1\left[\tilde{h}\Big(\frac{1}{J}\frac{\mathrm{D}^{\mathrm{s}}}{\mathrm{D}t}(J\tilde{n}^{\mathrm{f}})-{}_4\boldsymbol{\nabla}\cdot({}_4\mathbf{F}\cdot{}_4\tilde{\mathbf{K}}\cdot{}_4\boldsymbol{\nabla}_0\tilde{\mu}^{\mathrm{f}})\Big)\right]\mathrm{d}x_0\,\mathrm{d}V=0 \tag{25}$$

where $\tilde{h}$ is an arbitrary scalar function defined in each point of the hierarchy in V. Applying Gauss' theorem to (25) and transforming it to the reference configuration yields

$$\int_{V_0}\int_0^1\left[\tilde{h}\frac{\partial(J\tilde{n}^{\mathrm{f}})}{\partial(\tilde{\mu}^{\mathrm{f}}-p)}\frac{\mathrm{D}^{\mathrm{s}}}{\mathrm{D}t}(\tilde{\mu}^{\mathrm{f}}-p)+J({}_4\boldsymbol{\nabla}_0\tilde{h})\cdot{}_4\tilde{\mathbf{K}}\cdot{}_4\boldsymbol{\nabla}_0\tilde{\mu}^{\mathrm{f}}\right]\mathrm{d}x_0\,\mathrm{d}V_0=\int_{{}_4A_0}(J\tilde{h}\,{}_4\tilde{\mathbf{q}}_0)\mathrm{d}_4A_0 \tag{26}$$

Here ${}_4\tilde{\mathbf{q}}_0=({}_4\tilde{\mathbf{K}}\cdot{}_4\boldsymbol{\nabla}_0\tilde{\mu}^{\mathrm{f}})\cdot{}_4\tilde{\mathbf{n}}_0$ is the external flow through the hyper surface ${}_4A_0$ surrounding the hyper volume spanned by V and the hierarchical range $0\leqslant x_0\leqslant 1$, with four-dimensional normal ${}_4\tilde{\mathbf{n}}_0$.

Because the model describes finite deformations of a physically non-linear material, equations (19), (22) and (26) are non-linear and cannot be solved directly. Their solution is expressed by a three-dimensional displacement field for the solid $\mathbf{u}(\mathbf{x})$ ($v_0^{\mathrm{s}}=0$; equation (8)), a three-dimensional pressure field $p(\mathbf{x})$ (also p is x_0 independent), and a four-dimensional fluid pressure field which is represented by the fluid's chemical potential $\tilde{\mu}^{\mathrm{f}}(\mathbf{x},x_0)$. This solution is assumed to consist of an estimate, marked by $\hat{}$, and a perturbation, marked by δ:

$$\mathbf{u}=\hat{\mathbf{u}}+\delta\mathbf{u} \tag{27}$$

$$p=\hat{p}+\delta p \tag{28}$$

$$\tilde{\mu}^{\mathrm{f}}=\hat{\tilde{\mu}}^{\mathrm{f}}+\delta\tilde{\mu}^{\mathrm{f}} \tag{29}$$

Assuming that the perturbations are small compared to the estimates, the following expressions for the dependent variables can be derived:

$$\mathbf{F}=\hat{\mathbf{F}}+\delta\mathbf{F},\quad \hat{\mathbf{F}}=(\boldsymbol{\nabla}_0\hat{\mathbf{u}})^{\mathrm{c}},\quad \delta\mathbf{F}=(\boldsymbol{\nabla}_0\delta\mathbf{u})^{\mathrm{c}} \tag{30}$$

$$\mathbf{F}^{-1}\approx\hat{\mathbf{F}}^{-1}-\hat{\mathbf{F}}^{-1}\cdot\delta\mathbf{F}\cdot\hat{\mathbf{F}}^{-1} \tag{31}$$

$$J=\hat{J}+\delta J,\quad \hat{J}=\det(\hat{\mathbf{F}}),\quad \delta J=\det(\hat{\mathbf{F}})\hat{\mathbf{F}}^{-1}:\delta\mathbf{F} \tag{32}$$

$$\mathbf{E}=\hat{\mathbf{E}}+\delta\mathbf{E},\quad \delta\mathbf{E}=\hat{\mathbf{F}}^{\mathrm{c}}\cdot\delta\mathbf{F} \tag{33}$$

$$\mathbf{S}=\hat{\mathbf{S}}+\delta\mathbf{S},\quad \delta\mathbf{S}=\frac{\partial\mathbf{S}}{\partial\mathbf{E}}:(\hat{\mathbf{F}}^{\mathrm{c}}\cdot\delta\mathbf{F}) \tag{34}$$

Substitution of these variables into the weighted residual equations yields after linearization for the momentum equation (19):

$$\int_{V_0} (\nabla_0 \mathbf{f})^{\mathrm{c}} : \left[\left(\hat{\mathbf{S}} \cdot \delta \mathbf{F}^{\mathrm{c}} + \left(\frac{\partial \mathbf{S}}{\partial \mathbf{E}} : (\hat{\mathbf{F}}^{\mathrm{c}} \cdot \delta \mathbf{F}) \right) \cdot \hat{\mathbf{F}}^{\mathrm{c}} \right) - (\delta p \hat{J} \hat{\mathbf{F}}^{-1} + \hat{p} \delta J \hat{\mathbf{F}}^{-1} - \hat{p} \hat{J} \hat{\mathbf{F}}^{-1} \cdot \delta \mathbf{F} \cdot \hat{\mathbf{F}}^{-1}) \right] \mathrm{d}V_0$$
$$= - \int_{A_0} \hat{J} \mathbf{f} \cdot (\hat{\mathbf{F}}^{-\mathrm{c}} \cdot \mathbf{a}_0) \mathrm{d}A_0 + \int_{V_0} (\nabla_0 \mathbf{f})^{\mathrm{c}} : (-\hat{\mathbf{S}} \cdot \hat{\mathbf{F}}^{\mathrm{c}} + \hat{p} \hat{J} \hat{\mathbf{F}}^{-1}) \mathrm{d}V_0 \tag{35}$$

in which the two last terms on the left-hand side will be neglected. The linearized equation for conservation of solid mass (22) results in

$$\int_{V_0} g \left[\int_0^1 \tilde{c} \; \delta \dot{\tilde{\mu}}^{\mathrm{f}} \mathrm{d}x_0 - \int_0^1 \tilde{c} \mathrm{d}x_0 \; \delta \dot{p} - \hat{J} \hat{\mathbf{F}}^{-\mathrm{c}} \cdot \nabla_0 \cdot \delta \dot{\mathbf{u}} + \hat{J} \hat{\mathbf{F}}^{-\mathrm{c}} \cdot \delta \mathbf{F}^{\mathrm{c}} \cdot \hat{\mathbf{F}}^{-\mathrm{c}} \cdot \nabla_0 \cdot \hat{\mathbf{u}} - (\hat{J} \hat{\mathbf{F}}^{-1} : \delta \mathbf{F}) \hat{\mathbf{F}}^{-\mathrm{c}} \cdot \nabla_0 \cdot \hat{\mathbf{u}} \right] \mathrm{d}V_0$$
$$= \int_{V_0} g \left[- \int_0^1 \tilde{c} \; \hat{\dot{\tilde{\mu}}}^{\mathrm{f}} \mathrm{d}x_0 + \int_0^1 \tilde{c} \mathrm{d}x_0 \; \hat{\dot{p}} + \hat{J} \hat{\mathbf{F}}^{-\mathrm{c}} \cdot \nabla_0 \cdot \hat{\dot{\mathbf{u}}} \right] \mathrm{d}V_0 \tag{36}$$

in which vessel compliance $\tilde{c} = \partial(J\tilde{n}^{\mathrm{f}})/\partial(\tilde{\mu}^{\mathrm{f}} - p)$ represents the distensibility of the blood compartment (23) and the definition $\dot{\mathbf{u}} = (\mathrm{D}^{\mathrm{s}}\mathbf{u})/(\mathrm{D}t) = \mathbf{v}^{\mathrm{s}}$ has been used. The fourth and fifth terms on the left-hand side of this equation will be neglected. Similar to conservation of solid mass, conservation of fluid mass (26) is linearized:

$$\int_{V_0} \int_0^1 [\tilde{h}\tilde{c}(\delta \dot{\tilde{\mu}}^{\mathrm{f}} - \delta \dot{p}) + \hat{J}({}_4\nabla_0 \tilde{h}) \cdot {}_4\tilde{\mathbf{K}} \cdot {}_4\nabla_0 \delta \tilde{\mu}^{\mathrm{f}} + \hat{J} \hat{\mathbf{F}}^{-1} : \delta \mathbf{F} ({}_4\nabla_0 \tilde{h}) \cdot {}_4\tilde{\mathbf{K}} \cdot {}_4\nabla_0 \hat{\tilde{\mu}}^{\mathrm{f}}] \mathrm{d}x_0 \, \mathrm{d}V_0 = \int_{{}_4A_0} \tilde{h} \hat{J}_4 \tilde{\mathbf{q}}_0 \mathrm{d}_4 A_0$$
$$- \int_{V_0} \int_0^1 [\tilde{h}\tilde{c}(\hat{\dot{\tilde{\mu}}}^{\mathrm{f}} - \hat{\dot{p}}) + \hat{J}({}_4\nabla_0 \tilde{h}) \cdot {}_4\tilde{\mathbf{K}} \cdot {}_4\nabla_0 \hat{\tilde{\mu}}^{\mathrm{f}}] \mathrm{d}x_0 \, \mathrm{d}V_0 \tag{37}$$

where the third term of the left-hand side will be neglected. The simplifications that were introduced by neglecting several terms on the left-hand sides of the linearized equations are justified because the left-hand side terms are only involved in the estimation step of the non-linear computation.

3.2. Discretization

The linearized weighted residual equations for momentum (35), solid mass (36) and fluid mass (37) describe momentaneous equilibrium for a three-dimensional continuum, externally loaded by a force $\mathbf{a}$ and a flow ${}_4\tilde{\mathbf{q}}$. They cannot be solved exactly for each material point in the continuum. However, their exact solution can be approximated by interpolation of the solution that is calculated in a limited number of material points in the continuum, the nodal points. This approximated solution of the independent variables is expressed as

$$\mathbf{u}(\xi, t) = \phi^I(\xi) \mathbf{u}^I(t) = \phi^I(\xi) u_i^I(t) \mathbf{e}_i, \qquad I = 1, \ldots, n_u, \;\; i = 1, 2, 3 \tag{38}$$
$$p(\xi, t) = \varphi^J(\xi) p^J(t), \qquad J = 1, \ldots, n_p \tag{39}$$
$$\tilde{\mu}^{\mathrm{f}}(\tilde{\xi}, t) = \tilde{\chi}^K(\tilde{\xi}) \tilde{\mu}^{f^K}(t), \qquad K = 1, \ldots, \tilde{n}_{\mu^{\mathrm{f}}} \tag{40}$$

where Einstein summation convention is used and an orthonormal co-ordinate system has been introduced with unit vectors $\mathbf{e}_1$, $\mathbf{e}_2$ and $\mathbf{e}_3$. Here the interpolation functions ϕ^I and φ^J are defined in the material points ξ of the volume V, and $\tilde{\chi}^K$ is defined for the total hierarchical range in each of these material points, which is denoted as $\tilde{\xi} = (\xi, \xi_0)$. These interpolation functions are chosen such that they equal 1 in only one of the nodal points and that they equal 0 in all the other:

$$\phi^I(\xi^J) = \delta^{IJ} \tag{41}$$

$$\varphi^I(\xi^J) = \delta^{IJ} \tag{42}$$

$$\tilde{\chi}^I(\tilde{\xi}^J) = \delta^{IJ} \tag{43}$$

The number of interpolation functions therefore is equal to the corresponding number of nodal points: n_u for the displacements (ϕ^I), n_p for the hydrostatic pressure (φ^J) and $\tilde{n}_{\mu^{\mathrm{f}}}$ for the fluid pressure ($\tilde{\chi}^K$). According to Galerkin's method the weighting functions are chosen equal to the interpolation functions:[14]

$$\mathbf{f} \to \mathbf{f}_i^I = \phi^I \mathbf{e}_i, \qquad I = 1, \ldots, n_u, \;\; i = 1, 2, 3 \tag{44}$$

$$g \to g^J = \varphi^J, \qquad J = 1, \ldots, n_p \tag{45}$$

$$\tilde{h} \to \tilde{h}^K = \tilde{\chi}^K, \qquad K = 1, \ldots, \tilde{n}_{\mu^{\mathrm{f}}} \tag{46}$$

The gradient operator is discretized by

$$\mathbf{b}^I(\xi) = \boldsymbol{\nabla}_0 \phi^I(\xi) \tag{47}$$

$$\mathbf{c}^J(\xi) = \boldsymbol{\nabla}_0 \varphi^J(\xi) \tag{48}$$

$${}_4\tilde{\mathbf{d}}^K(\tilde{\xi}) = {}_4\boldsymbol{\nabla}_0 \tilde{\chi}^K(\tilde{\xi}) \tag{49}$$

Thus, the gradients of the weighting functions are written as

$$\boldsymbol{\nabla}_0 \mathbf{f}_i^I = \mathbf{b}^I \mathbf{e}_i \tag{50}$$

$$\boldsymbol{\nabla}_0 g^J = \mathbf{c}^J \tag{51}$$

$${}_4\boldsymbol{\nabla}_0 \tilde{h}^K = {}_4\tilde{\mathbf{d}}^K \tag{52}$$

The discretized weighted residual equations are written in matrix form. This matrix equation consists of a damping part, a stiffness part and a right hand side which represents the difference between the external loads and internal loads:

$$\begin{bmatrix} 0 & 0 & 0 \\ {}^{u}_{\mathrm{s}}B^{JL}_{j} & {}^{p}_{\mathrm{s}}B^{JM} & {}^{\mu^{\mathrm{f}}}_{\mathrm{s}}B^{JN} \\ 0 & {}^{p}_{\mathrm{f}}B^{KM} & {}^{\mu^{\mathrm{f}}}_{\mathrm{f}}B^{KN} \end{bmatrix} \begin{Bmatrix} \delta \dot{u}_j^L \\ \delta \dot{p}^M \\ \delta \dot{\tilde{\mu}}^{\mathrm{f}\,N} \end{Bmatrix} + \begin{bmatrix} {}^{u}_{\mathrm{m}}K^{IL}_{ij} & {}^{p}_{\mathrm{m}}K^{IM}_{i} & 0 \\ 0 & 0 & 0 \\ 0 & 0 & {}^{\mu^{\mathrm{f}}}_{\mathrm{f}}K^{KN} \end{bmatrix} \begin{Bmatrix} \delta u_j^L \\ \delta p^M \\ \delta \tilde{\mu}^{\mathrm{f}\,N} \end{Bmatrix} = \begin{Bmatrix} {}_{\mathrm{m}}R^I_{\mathrm{ex}\,i} \\ 0 \\ {}_{\mathrm{f}}\tilde{R}^K_{\mathrm{ex}} \end{Bmatrix} - \begin{Bmatrix} {}_{\mathrm{m}}R^I_{\mathrm{in}\,i} \\ {}_{\mathrm{s}}R^J_{\mathrm{in}} \\ {}_{\mathrm{f}}\tilde{R}^K_{\mathrm{in}} \end{Bmatrix} \tag{53}$$

The upper and lower left-indices of the matrix elements refer to the corresponding degree of freedom ($\mathbf{u}$, p or $\tilde{\mu}^{\mathrm{f}}$) and the corresponding equation (conservation of momentum, solid mass or fluid mass), respectively. The upper and lower right indices refer to row number (I, J, K) and

column number (L,M,N), and to displacement component j, respectively. The ranges of the right indices are: $I,L = 1,\ldots,n_u$; $J,M = 1,\ldots,n_p$; $K,N = 1,\ldots,\tilde{n}_{\mu^{\mathrm{f}}}$; $j = 1,2,3$. The matrix elements are

$$ {}^{u}_{\mathrm{m}}K^{IL}_{ij} = \int_{V_0} \left[\mathbf{e}_i \mathbf{b}^I : \hat{\mathbf{S}} \cdot \mathbf{b}^L \mathbf{e}_j + (\mathbf{e}_i \mathbf{b}^I \cdot \hat{\mathbf{F}}^{\mathrm{c}}) : \left(\frac{\partial \mathbf{S}}{\partial \mathbf{E}} \right) : (\mathbf{e}_j \mathbf{b}^L \cdot \hat{\mathbf{F}}^{\mathrm{c}}) \right] \mathrm{d}V_0 \tag{54} $$

$$ {}^{p}_{\mathrm{m}}K^{IM}_{i} = -\int_{V_0} (\hat{\mathbf{F}}^{-\mathrm{c}} : \mathbf{b}^I \mathbf{e}_i \varphi^M) \hat{J} \, \mathrm{d}V_0 \tag{55} $$

$$ {}^{u}_{\mathrm{s}}B^{JL}_{j} = \int_{V_0} (\varphi^J \hat{\mathbf{F}}^{-\mathrm{c}} : \mathbf{b}^L \mathbf{e}_j) \hat{J} \, \mathrm{d}V_0 \tag{56} $$

$$ {}^{p}_{\mathrm{s}}B^{JM} = \int_{V_0} \left(\varphi^J \int_0^1 \tilde{c} \, \mathrm{d}x_0 \varphi^M \right) \mathrm{d}V_0 \tag{57} $$

$$ {}^{\mu^{\mathrm{f}}}_{\mathrm{s}}B^{JN} = -\int_{V_0} \left(\varphi^J \int_0^1 \tilde{c} \;\; \tilde{\chi}^N \, \mathrm{d}x_0 \right) \mathrm{d}V_0 \tag{58} $$

$$ {}^{p}_{\mathrm{f}}B^{KM} = -\int_{V_0} \left(\int_0^1 \tilde{\chi}^K \tilde{c} \, \mathrm{d}x_0 \;\; \varphi^M \right) \mathrm{d}V_0 \tag{59} $$

$$ {}^{\mu^{\mathrm{f}}}_{\mathrm{f}}B^{KN} = \int_{V_0} \left(\int_0^1 \tilde{\chi}^K \tilde{c} \;\; \tilde{\chi}^N \, \mathrm{d}x_0 \right) \mathrm{d}V_0 \tag{60} $$

$$ {}^{\mu^{\mathrm{f}}}_{\mathrm{f}}K^{KN} = \int_{V_0} \left(\int_0^1 \tilde{\mathbf{d}}^K \cdot {}_4\tilde{\mathbf{K}} \cdot \tilde{\mathbf{d}}^N \, \mathrm{d}x_0 \right) \hat{J} \, \mathrm{d}V_0 \tag{61} $$

$$ {}_{\mathrm{m}}R^{I}_{\mathrm{ex}i} = -\int_{A_0} (\phi^I \mathbf{e}_i \cdot \hat{\mathbf{F}}^{-\mathrm{c}} \cdot \mathbf{a}_0) \hat{J} \, \mathrm{d}A_0 \tag{62} $$

$$ {}_{\mathrm{f}}\tilde{R}^{K}_{\mathrm{ex}} = \int_{4A_0} \tilde{\chi}^K {}_4\tilde{\mathbf{q}} \hat{J} \, \mathrm{d}_4 A_0 \tag{63} $$

$$ {}_{\mathrm{m}}R^{I}_{\mathrm{in}i} = \int_{V_0} \hat{\mathbf{S}} : \hat{\mathbf{F}}^{\mathrm{c}} \cdot \mathbf{e}_i \mathbf{b}^I \, \mathrm{d}V_0 + {}^{p}_{m}K^{IM}_{i} \hat{p}^M \tag{64} $$

$$ {}_{\mathrm{s}}R^{J}_{\mathrm{in}} = \left[{}^{u}_{\mathrm{s}}B^{JL} \;\; {}^{p}_{\mathrm{s}}B^{JM} \;\; {}^{\mu^{\mathrm{f}}}_{\mathrm{s}}B^{JN} \right] \begin{Bmatrix} \hat{u}^L_j \\ \hat{p}^M \\ \hat{\tilde{\mu}}^{\mathrm{f}N} \end{Bmatrix} \tag{65} $$

$$ {}_{\mathrm{f}}\tilde{R}^{K}_{\mathrm{in}} = \left[{}^{p}_{\mathrm{f}}B^{KM} \;\; {}^{\mu^{\mathrm{f}}}_{\mathrm{f}}B^{KN} \;\; {}^{\mu^{\mathrm{f}}}_{\mathrm{f}}K^{KN} \right] \begin{Bmatrix} \hat{p}^M \\ \hat{\tilde{\mu}}^{\mathrm{f}N} \\ \hat{\tilde{\mu}}^{\mathrm{f}N} \end{Bmatrix} \tag{66} $$

3.3. Implementation

Because finite element programs and their pre and post-processors generally deal with up to three-dimensional elements, the integration over the x_0 range is implicitly performed within each spatial node. For this purpose the four-dimensional interpolation function $\tilde{\chi}$ is split into two independent parts: one three-dimensionally defined part χ, which is expressed as a function of the

three-dimensional co-ordinates $\mathbf{x}$ of the material points $\tilde{\xi}$, and a part χ_0 that only depends on the x_0 co-ordinate of the material points $\tilde{\xi}$. Thus, the four-dimensional solution of $\tilde{\mu}^{\mathrm{f}}$ is rewritten:

$$\tilde{\mu}^{\mathrm{f}}(\tilde{\xi},t) = \chi_{0_k}(x_0)\chi^K(\mathbf{x})\tilde{\mu}_k^{f^K}(t), \quad K = 1,\ldots,n_{\mu^{\mathrm{f}}}, \quad k = 1,\ldots,n_0 \tag{67}$$

The original four-dimensional set of nodal points $\tilde{\xi}^J; J = 1,\ldots,\tilde{n}_{\mu^{\mathrm{f}}}$, is split into n_0 three-dimensional sets of nodal points $\xi^K; K = 1,\ldots,n_{\mu^{\mathrm{f}}}$, where each of these sets has a different x_0 value. Obviously, $\tilde{n}_{\mu^{\mathrm{f}}} = n_0\ n_{\mu^{\mathrm{f}}}$. The integrations over x_0 in the matrix elements (57), (58), (59), (60) and (61), are included as algebraic expressions, that result from the integrations over the x_0 range, in the element matrix:

$$\overset{p}{\mathrm{s}}B^{JM} = \int_{V_0} (\varphi^J C \varphi^M)\,\mathrm{d}V_0, \quad C = \int_0^1 \tilde{c}\,\mathrm{d}x_0 \tag{68}$$

$$\overset{\mu^{\mathrm{f}}}{\mathrm{s}}B_n^{JN} = -\int_{V_0} (\varphi^J c_n\ \chi^N)\,\mathrm{d}V_0, \quad c_n = \int_0^1 \tilde{c}\chi_{0_n}\,\mathrm{d}x_0 \tag{69}$$

$$\overset{p}{\mathrm{f}}B_k^{KM} = -\int_{V_0} (\chi^K{}_k c\ \varphi^M)\,\mathrm{d}V_0, \quad {}_k c = \int_0^1 \chi_{0_k}\ \tilde{c}\,\mathrm{d}x_0 \tag{70}$$

$$\overset{\mu^{\mathrm{f}}}{\mathrm{f}}B_{kn}^{KN} = \int_{V_0} (\chi^K{}_k c_n\,\chi^N)\,\mathrm{d}V_0, \quad {}_k c_n = \int_0^1 \chi_{0_k}\ \tilde{c}\,\chi_{0_n}\,\mathrm{d}x_0 \tag{71}$$

$$\begin{aligned}\overset{\mu^{\mathrm{f}}}{\mathrm{f}}K_{kn}^{KN} = \int_{V_0} (&\chi^K{}_k k_{00_n}\chi^N + \chi^K{}_k\mathbf{k}_{0_n}\cdot\boldsymbol{\nabla}_0\chi^N \\ &+\boldsymbol{\nabla}_0\chi^K\cdot{}_n\mathbf{k}_{0k}\chi^N + \boldsymbol{\nabla}_0\chi^K\cdot{}_k\mathbf{K}_n\cdot\boldsymbol{\nabla}_0\chi^N)\,\hat{J}\,\mathrm{d}V_0\end{aligned} \tag{72}$$

$$\begin{aligned}{}_k k_{00_n} &= \int_0^1 \frac{\partial\chi_{0_k}}{\partial x_0}\tilde{k}_{00}\frac{\partial\chi_{0_n}}{\partial x_0}\,\mathrm{d}x_0, \quad {}_k\mathbf{k}_{0_n} = \int_0^1 \frac{\partial\chi_{0_k}}{\partial x_0}\ \tilde{\mathbf{k}}_0\chi_{0_n}\,\mathrm{d}x_0 \\ {}_n\mathbf{k}_{0k} &= \int_0^1 \chi_{0_k}\ \tilde{\mathbf{k}}_0\frac{\partial\chi_{0_n}}{\partial x_0}\,\mathrm{d}x_0, \quad {}_k\mathbf{K}_n = \int_0^1 \chi_{0_k}\,\tilde{\mathbf{K}}\chi_{0_n}\,\mathrm{d}x_0\end{aligned}$$

In all the above definitions the ranges of the indices are

$$J,M = 1,\ldots,n_p, \quad K,N = 1,\ldots,n_{\mu^{\mathrm{f}}}, \quad k,n = 1,\ldots,n_0. \tag{73}$$

The definition of ${}_4\tilde{\mathbf{K}}$ according to (11) has been used and it should be noted that $\tilde{k}_{00}$, $\tilde{\mathbf{k}}_0$ and $\tilde{\mathbf{K}}$ depend on x_0. The one-dimensional interpolation functions χ_{0_k} are linear functions of x_0. Because of the structure of the software package DIANA, the spatial interpolation functions χ^K are chosen equal to the spatial interpolation functions ϕ^K and φ^K. Their shape can be linear or quadratic.[15] The solutions for u_i^K, p^K and $\tilde{\mu}_j^{f^K}$ are calculated in the same spatial nodal points ξ^K, and $n_u = n_p = n_{\mu^{\mathrm{f}}}$. The input parameters $\tilde{c}$ and ${}_4\tilde{\mathbf{K}}$ are constant per element in the x_0 range. The number of elements in the x_0 range may vary between 1 and 5 ($2 \leqslant n_0 \leqslant 6$).

Time discretization is achieved by a third-order Houbolt scheme, which defines the time derivative of the independent variables as a function of their actual value and their values at three previous time steps:[14]

$$\dot{s}(t) = h_0 s(t) + \sum_{i=1}^{3} h_i s(t-\tau_i), \quad s = u_j, p, \tilde{\mu}^{\mathrm{f}} \tag{74}$$

Thus, time derivative of the iterative change δs can be expressed as $\delta\dot{s}(t) = h_0\delta s(t)$. Consequently, the resulting total element matrix after time integration can be written as $\mathbf{K}^{\mathrm{tot}} = [h_0\mathbf{B}^{\mathrm{el}} + \mathbf{K}^{\mathrm{el}}]$ where

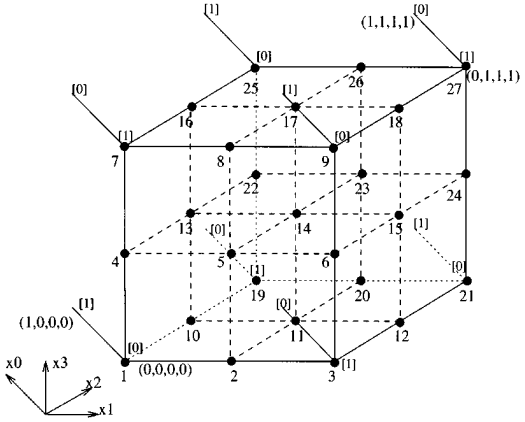

Figure 2. Mesh with boundary conditions and node numbers used in finite element simulation of the four-dimensional Laplace problem. The oblique lines in the nodes represent the hierarchical range, where $x_0 = 0$ at the node and $x_0 = 1$ at the other end of the line. The values of the nodal boundary conditions for the fluid pressures at $x_0 = 0$ and $x_0 = 1$ are printed between rectangular brackets

$\mathbf{B}^{\mathrm{el}}$ is the element damping matrix and $\mathbf{K}^{\mathrm{el}}$ is the element stiffness matrix (53). Because symmetry can be found in the element submatrices ${}^{p}_{\mathrm{s}}\mathbf{B}$, ${}^{\mu^{\mathrm{f}}}_{\mathrm{f}}\mathbf{B}$, ${}^{u}_{\mathrm{m}}\mathbf{K}$, ${}^{\mu^{\mathrm{f}}}_{\mathrm{f}}\mathbf{K}$ and moreover ${}^{p}_{\mathrm{f}}B^{KM}_{k} = {}^{\mu^{\mathrm{f}}}_{\mathrm{s}}B^{MK}_{k}$ and ${}^{u}_{\mathrm{s}}B^{JL}_{j} = -{}^{p}_{\mathrm{m}}K^{LJ}_{j}$, the element matrix $\mathbf{K}^{\mathrm{tot}}$ can be reordered to symmetry.

In simulations physically non-linear material behaviour is included, as well as geometrical non-linearity. The resulting non-linear system of equations is solved by a regular or modified Newton–Raphson technique and Gauss decomposition.[16]

4. TESTS

4.1. Laplace equation

The finite element model describes four-dimensional fluid flow through distensible pores in a deforming porous solid. This process is governed by equations (14)–(16). If solid deformation and pore distensibility are suppressed, $\boldsymbol{\sigma}^{\mathrm{eff}}$ in (14), and $\mathbf{v}^{\mathrm{s}}$ and $(\partial \tilde{n}^{\mathrm{f}})/(\partial t)$ in (15) and (16) disappear. The resulting governing equation is

$$ {}_4\boldsymbol{\nabla} \cdot {}_4\tilde{\mathbf{K}} \cdot {}_4\boldsymbol{\nabla} \tilde{\mu}^{\mathrm{f}} = 0 \tag{75} $$

in which the Laplace equation can be recognized if ${}_4\tilde{\mathbf{K}}$ is constant in the considered domain.

To test the implementation of the model, the above described problem has been analysed and the solution was compared to an analytical solution of the four-dimensional Laplace equation. Figure 2 shows the three-dimensional mesh with the four-dimensional boundary conditions for the fluid pressure $\tilde{\mu}^{\mathrm{f}}$. Nodal displacements were suppressed and the permeability tensor equalled the identity tensor: ${}_4\tilde{\mathbf{K}} = {}_4\mathbf{I}$. Vessel compliance was very low: $\tilde{c} = 0{\cdot}001$. The x_0 range was discretized by 4 linear elements and each of the 5 fluid pressures was prescribed in the corners of the geometry, as indicated in Figure 2.

This problem is defined by the following equation:

$$ {}_4\boldsymbol{\nabla}^2 \tilde{\mu}^{\mathrm{f}} = 0, \quad \tilde{\mu}^{\mathrm{f}} = \tilde{\mu}^{\mathrm{f}}(x_0, x_1, x_2, x_3), \quad 0 \leqslant x_i \leqslant 1, \ \ i = 0, 1, 2, 3 \tag{76} $$

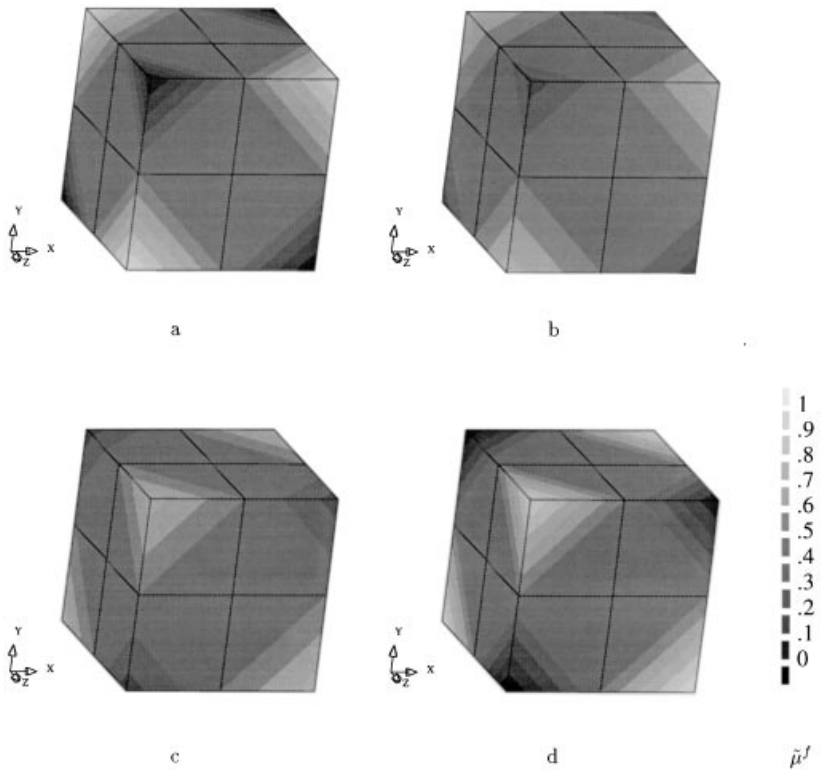

Figure 3. Numerical solution of the four-dimensional Laplace equation; respectively first, second, fourth and fifth fluid pressure pattern on the three-dimensional body (a, b, c, d)

with boundary conditions (Figure 2)

$$\tilde{\mu}^{\mathrm{f}}(x_0, \mathbf{x}) = x_0, \quad \mathbf{x} = \left\{ \begin{matrix} 0 \\ 0 \\ 0 \end{matrix} \right\}, \left\{ \begin{matrix} 1 \\ 1 \\ 0 \end{matrix} \right\}, \left\{ \begin{matrix} 1 \\ 0 \\ 1 \end{matrix} \right\}, \left\{ \begin{matrix} 0 \\ 1 \\ 1 \end{matrix} \right\} \tag{77}$$

$$\tilde{\mu}^{\mathrm{f}}(x_0, \mathbf{x}) = 1 - x_0, \quad \mathbf{x} = \left\{ \begin{matrix} 1 \\ 0 \\ 0 \end{matrix} \right\}, \left\{ \begin{matrix} 0 \\ 1 \\ 0 \end{matrix} \right\}, \left\{ \begin{matrix} 0 \\ 0 \\ 1 \end{matrix} \right\}, \left\{ \begin{matrix} 1 \\ 1 \\ 1 \end{matrix} \right\} \tag{78}$$

$$\mathbf{x} = \left\{ \begin{matrix} x_1 \\ x_2 \\ x_3 \end{matrix} \right\}$$

An analytical solution of this equation is expressed as:

$$\begin{aligned} \tilde{\mu}^{\mathrm{f}} = {} & x_0 + x_1 + x_2 + x_3 \\ & - 2x_0x_1 - 2x_0x_2 - 2x_0x_3 - 2x_1x_2 - 2x_1x_3 - 2x_2x_3 \\ & + 4x_0x_1x_2 + 4x_0x_2x_3 + 4x_1x_2x_3 + 4x_0x_1x_3 - 8x_0x_1x_2x_3 \end{aligned} \tag{79}$$

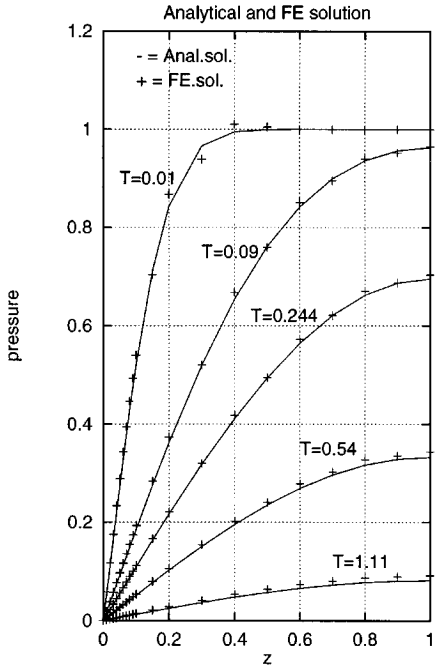

Figure 4. Analytical[17] and numerical (FE) solution of the one-dimensional linear confined compression test

The computed numerical solutions of each fluid pressure appeared to be equal to the corresponding analytical solutions in each nodal point. The computed solution is presented as a number of contour plots of fluid pressures, each representing a different hierarchical position, on the surface of the three-dimensional body $0 \leqslant x_i \leqslant 1;\ i = 1,2,3$ (Figure 3).

4.2. *Confined compression*

The poroelastic behaviour of the model is tested by comparing numerical results for the fluid pressure in a confined compression test to an analytical solution.[17] In the simulation a cylindrical, hierarchically porous sample with cross-sectional surface of 1 mm^2, height of 1 mm, Young modulus of 100 N/mm^2, Poisson ratio of 0·3, and axial permeability $k_{zz} = 0{\cdot}00743\,\mathrm{mm}^4/(\mathrm{N\,s})$, is loaded by a force of $-1N$ on the top surface ($z = 1$), while the bottom surface ($z = 0$) is supported by a highly permeable filter ($p = 0$). Vessel compliance is chosen very large, $\tilde{c} = 1000$, so that all fluid pressures equal hydrostatic pressure, and a biphasic mixture behaviour is approximated. The mesh consists of 10 quadratic axisymmetric elements and the x_0 range is discretized by 1 linear element. Nodal pressures and analytical solution are plotted against their z-co-ordinate at several points in time (T) (Figure 4).

5. APPLICATION

The finite element model can be used to simulate finite deformations of, and fluid flow through, hierarchically arranged porous solids. A simulation of blood perfusion in a non-contracting, three-dimensional model of a rat calf muscle (medial gastrocnemius) is presented by Vankan *et al.*[18]

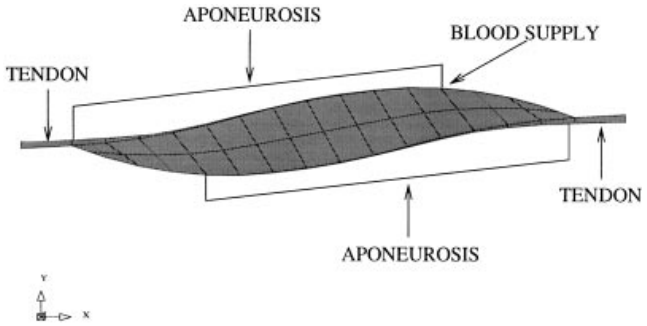

Figure 5. Finite element muscle model geometry. The mesh consists of 52 2-D 8-node quadratic plane strain elements; 28 for the muscle belly, 22 for the aponeuroses and 2 for the tendons. Displacements in all directions of the free ends of the tendons are suppressed, and arterial and venous blood pressure are prescribed in one node

A strongly simplified model of the same muscle is used here in a simulation of blood perfusion during contraction.

5.1. Input

The 3-D muscle geometry is modelled by a 2-D plane strain approximation. The simplified model geometry and mesh are given in Figure 5. The mesh consists of 28 2-D 8-node quadratic plane strain elements for the muscle belly, and 24 of the same elements for the tendons and aponeuroses (tendinous sheets on the muscle surface by which the tendons are attached to the muscle). The muscle belly is 5 mm wide (Y-direction) and 30 mm long (X-direction). The tendons are 3 mm long and 0·1 mm thick and consist of one element each. The aponeuroses, each consisting of 11 elements, are 22 mm long and run in thickness from 0·1 mm at the tendon to 0 mm at the other end.

The tendinous material of tendons and aponeuroses was assumed to behave linearly elastic with a Young modulus of 1·5 GPa[19] and Poisson ratio of 0·3. The mechanical behaviour of the passive muscle material is based on a description of cardiac tissue by Bovendeerd.[20] It is non-linearly elastic and transversely isotropic with respect to the muscle fibers. Thus, the contribution of the Green–Lagrange strain tensor $\mathbf{E}$ to the elastic energy W, is expressed as

$$W_{\mathrm{E}} = C[e^{a(2E_{11}^2+E_{22}^2+2E_{12}^2)} - 1] \tag{80}$$

where $C = 0{\cdot}7$ kPa, $a = 5{\cdot}0$. The indices $1, 2, 3$ correspond to the local element co-ordinate system with base vectors $\mathbf{e}_1, \mathbf{e}_2, \mathbf{e}_3$, where $\mathbf{e}_1$ coincides with the local fibre direction (Figure 5).

Contraction is modelled as an active component of the second Piola–Kirchhoff stress in the fibre direction. This contraction stress is defined as a function of time according to

$$S = S_{\max}\left[1 - \frac{1}{1 + (t/t_r)^4}\right] \tag{81}$$

where $S_{\max} = 100$ KPa, $t_{\mathrm{r}} = 50$ ms, and t is time in ms. The choice of the function and its parameters is roughly estimated from tetanic isometric force generation in rat gastrocnemius medialis muscle as described by Huijing and Rozendal.[21]

Blood perfusion is described as fluid flow through the hierarchical pores (vascular tree) of the muscle. The hierarchy was divided into 3 intercommunicating compartments (arterial, arteriolar and venous). Both spatial ($\tilde{\mathbf{K}}$) and hierarchical permeability ($\tilde{k}_{00}$) were prescribed for each of the

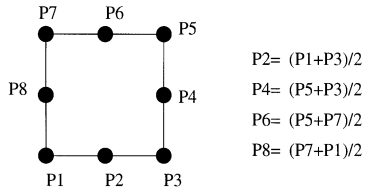

Figure 6. Linearizing pressure constraints in 8-node element that were prescribed for p and $\tilde{\mu}^{\mathrm{f}}$

Table I. Vascular parameters

	$\tilde{K}\left(\frac{mm^2}{\mathrm{s\ kPa}}\right)$	$\tilde{k}_{00}\left(\frac{1}{\mathrm{s\ kPa}}\right)$	$\tilde{c}\left(\frac{1}{\mathrm{kPa}}\right)$
Arterial	100	0·0025	0·001
Arteriolar	0·05	0·000325	0·001
Venous	100	0·0025	0·1

compartments. For the sake of simplicity the spatial permeability was taken isotropic and the three-dimensional permeability tensor was assumed to be diagonal: ${}_3\tilde{\mathbf{K}} = \tilde{k}_{00}\mathbf{e}_0\mathbf{e}_0 + \tilde{K}\mathbf{e}_i\mathbf{e}_i;\ i = 1,2$, where $\mathbf{e}_0$ is the base vector in x_0 direction. Moreover, ${}_3\tilde{\mathbf{K}}$ was assumed to depend only on hierarchical position, being constant within each compartment, and constant over the whole geometry. The actual values used in the simulation are listed in Table I.

Just like the permeability, the vessel compliance $\tilde{c}$ is assumed to depend only on hierarchical position, being constant within each compartment, and constant over the whole geometry. Its values are also listed in Table I. Because permeability and compliance do not depend on $\tilde{n}^{\mathrm{f}}$ in this simulation, the initial fluid volume fractions $\tilde{n}^{\mathrm{f}}_{t=0}$ do not appear in the equations and are not needed as input.

In order to prevent oscillations in the solution for the hydrostatic pressure p, it was necessary to reduce the order of interpolation for p and $\tilde{\mu}^{\mathrm{f}}$. This was achieved by adding constraints for these degrees of freedom: the values in each mid-side node were prescribed to equal the average of the values in the corresponding corner nodes (Figure 6).

The model contains 192 nodes, 76 of which have only 2 degrees of freedom (u_1, u_2) and the other 116 have 7 degrees of freedom $(u_1, u_2, p, \mu^{\mathrm{f}}_1, \mu^{\mathrm{f}}_2, \mu^{\mathrm{f}}_3, \mu^{\mathrm{f}}_4)$. Displacements of the nodes of the free ends of the tendons are suppressed, and μ^{f}_1 and μ^{f}_4 are prescribed in one node. Furthermore linearizing constraints were applied to each pressure in 72 midnodes. the resulting system consists of $76 \times 2 + 116 \times 7 - 6 \times 2 - 2 - 72 \times 5 = 590$ linearized equations, which were solved iteratively in 12 time steps.

5.2. *Results*

The simulation consists of two phases. In the first phase passive perfusion is calculated, which results from boundary conditions of 10 kPa arterial pressure and a 0 kPa venous pressure prescribed in one node in the tip of one aponeurosis at the muscle surface (Figure 5). This node can be interpreted as the position where the supplying arterial vessel enters the muscle, and the draining venous vessel leaves the muscle. Due to the prescribed arterial pressure and the permeability of the tissue, blood enters the muscle, arterial pressure rises in the whole geometry, blood flows towards the arteriolar and venous compartments so that blood pressures in these compartments also rise. After about 10 ms a stationary perfusion situation comes into being. A decay in blood pressure

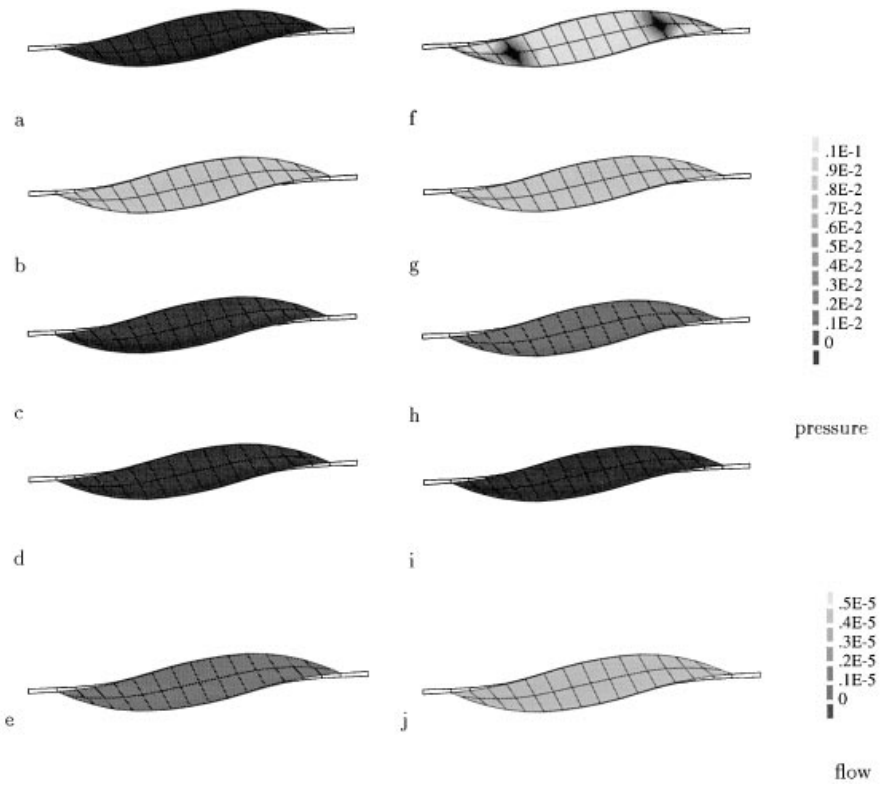

Figure 7. Contours of hydrostatic and blood pressures (MPa) and hierarchical flow (1/ms) in the passive and contracted muscle: (a) passive hydrostatic pressure; (b) passive arterial blood pressure; (c) passive capillary blood pressure; (d) passive venous blood pressure; (e) passive hierarchical blood flow at venular level; (f) hydrostatic pressure during contraction; (g) arterial blood pressure during contraction; (h) capillary blood pressure during contraction; (i) venous blood pressure during contraction; (j) hierarchical blood flow at venular level during contraction

from the arterial to the venous compartment is found. In Figures 7(b)–7(d) contour plots of these blood pressures are given. These values approximately correspond with blood pressures that were measured in skeletal muscles.[22]

Next contraction is started. Displacements of the free ends of the tendons are suppressed (isometric contraction). After 100 ms the contraction stress has reached its maximum (tetanic contraction). Due to this contraction stress, a strong rise in hydrostatic pressure occurs (Figure 7(f)), which is transmitted via the vessel walls particularly to the venous blood (Figure 7(h)), while the arterial blood pressure hardly changes (Figure 7(g)). Due to this increase in venous blood pressure, the blood is squeezed out of the muscle and a strongly increased hierarchical venous flow occurs (Figure 7(j)).

6. DISCUSSION

To the authors' knowledge, this is the first finite element formulation for the integrated description of finite deformation of and fluid flow through hierarchical porous media. A particular application of the finite element model is analysis of the mechanical interaction between deformation and blood perfusion of biological tissue. This interaction plays a significant role in, for example,

myocardial infarct or initial obstruction of perfusion during skeletal muscle contraction. This study focusses on phenomena in skeletal muscles, as was illustrated in the presented simulation. The rise in hydrostatic pressure during contraction of the muscle, as was predicted by the model, was qualitatively consistent with experimental findings of Kirkebø and Wisnes.[23] Some years earlier, the same authors reported a decrease in blood perfusion during contraction in the centre of the muscle,[24] which supports the concept of a mechanical link between tissue deformation and blood perfusion.

The presented finite element formulation is based on three equations: conservation of momentum for the mixture, conservation of solid mass and conservation of fluid mass. Both solid and fluid are incompressible, which is accounted for in their conservation equations. The solid displacements, hydrostatic pressure and fluid pressures are chosen as degrees of freedom, in order to keep the number of nodal degrees of freedom to a minimum.

In the implementation of the finite element model, the spatial interpolation functions for the displacements **u**, hydrostatic pressure p and fluid pressure $\tilde{\mu}^{\mathrm{f}}$, are of the same order. The finite element equations (53), however, imply that p should be interpolated one order lower than **u** (momentum equation) and spatial interpolation of $\tilde{\mu}^{\mathrm{f}}$ should be of the same order as of p (conservation of solid mass). Nevertheless, equal orders of spatial interpolation for all degrees of freedom have been used because of the structure of the DIANA-package. Calculations have shown numerical oscillations in the solution of the hydrostatic pressure p. Reducing the order of interpolation for p and $\tilde{\mu}^{\mathrm{f}}$ by linearizing constraints (Figure 6) resolved this problem.

REFERENCES

1. R. de Borst, G. M. A. Kusters, P. Nauta and F. C. de Witte, 'DIANA—a comprehensive, but flexible finite element system', in C. A. Brebbia (ed.), *Finite Element Systems: a Handbook*, Springer, Berlin, 1985.
2. J. Z. Livingston and J. R. Resar, 'Effect of tetanic myocardial contraction on coronary pressure-flow relationships', *Am. J. Physiol.*, **265,** H1215–H1226 (1993).
3. J. R. Resar, R. M. Judd, H. R. Halperin, V. P. Chacko, R. G. Weiss and F. C. P. Yin, 'Direct evidence that coronary perfusion affects diastolic myocardial mechanical properties in canine heart', *Cardiovasc. Res.*, **27,** 403–410 (1993).
4. C. W. J. Oomens, D. H. van Campen and H. J. Grootenboer, 'A mixture approach to the mechanics of skin', *J. Biomech.*, **20,** 877–885 (1987).
5. J. M. Huyghe, T. Arts, D. H. van Campen and R. S. Reneman, 'Porous medium finite element model of the beating left ventricle', *Am. J. Physiol.*, **262,** H1256–H1267 (1992).
6. M. A. Biot, 'Theory of finite deformations of porous solids', *Indiana Univ. Math. J.*, **21,** 597–620 (1972).
7. J. M. Huyghe and D. H. van Campen, 'Finite deformation theory of hierarchically arranged porous solids: I. Balance of mass and momentum', *Int. J. Eng. Sci.*, **33,** 1861–1871 (1995).
8. J. M. Huyghe and D. H. van Campen, 'Finite deformation theory of hierarchically arranged porous solids: II. Constitutive behaviour', *Int. J. Eng. Sci.*, **33,** 1873–1886 (1995).
9. J. M. Huyghe, C. W. Oomens, D. H. van Campen and R. M. Heethaar, 'Low Reynolds number steady state flow through a branching network of rigid vessels: I. A mixture theory', *Biorheology*, **26,** 55–71 (1989).
10. J. M. Huyghe, C. W. Oomens and D. H. van Campen, 'Low reynolds number steady state flow through a branching network of rigid vessels: II. A finite element mixture model', *Biorheology*, **26,** 73–84 (1989).
11. R. M. Bowen, 'Incompressible porous media models by use of the theory of mixtures', *Int. J. Eng. Sci.*, **18,** 1129–1148 (1980).
12. W. J. Vankan, J. M. Huyghe, J. D. Janssen and A. Huson, 'Poroelasticity of saturated solids with an application to blood perfusion', *Int. J. Eng. Sci.*, in press.
13. O. C. Zienkiewicz, *The Finite Element Method*, 3rd edn, McGraw-Hill, Maidenhead, 1977.
14. K. J. Bathe, *Finite Element Procedures in Engineering Analysis*, 1st edn, Prentice-Hall, Englewood Cliffs, N.J., 1982.
15. TNO Building and Construction Research Delft, The Netherlands, *DIANA User's Manual: Linear Static Analysis*, Release 5.1, Vol. 1, 1993.
16. TNO Building and Construction Research Delft, The Netherlands, *DIANA User's Manual: Non-linear Analysis*, Release 5.1, Vol. 4, 1993.
17. K. Terzaghi, *Theoretical Soil Mechanics*, Wiley, New York, 1943.
18. W. J. Vankan, J. M. Huyghe, J. D. Janssen and A. Huson, 'A 3-D finite element model of blood perfused rat gastrocnemius medialis muscle', *Eur. J. Morph.*, **34,** 19–24 (1996).
19. C. L. Trestik and R. L. Lieber, 'Relationship between achilles tendon mechanical properties and gastrocnemius muscle function', *J. Biomech. Eng.*, **115,** 225–230 (1993).

20. P. H. M. Bovendeerd, 'The mechanics of the normal and ischemic left ventricle during the cardiac cycle', Ph.D. dissertation, University of Limburg, Maastricht, The Netherlands, 1990.
21. P. A. J. B. M. Huijing and R. H. Rozendal, 'General myology', in R. H. Rozendal, P. A. J. B. M. Huijing, Y. F. Heerkens and R. D. Woittiez (eds.), *Introduction to Human Kinesiology*, Chapter 5, Educaboek BV, Culemborg, 1990, pp. 199–274 (in Dutch).
22. K. Fronek and B. W. Zweifach, 'Microvascular pressure distribution in skeletal muscle and the effect of vasodilation', *Am. J. Physiol.*, **228,** 791–796 (1975).
23. A. Kirkebø and A. Wisnes, 'Regional tissue fluid pressure in rat calf muscle during sustained contraction or stretch', *Acta Physiol. Scand.*, **114,** 551–556 (1982).
24. A. Wisnes and A. Kirkebø, 'Regional distribution of blood flow in calf muscles of rat during passive stretch and sustained contraction', *Acta Physiol. Scand.*, **96,** 256–266 (1976).